ALP explanation to the muon $(g-2)$ and its test at future Tera-Z and Higgs factories

Jia Liu,[1,2,†] Xiaolin Ma,[1,‡] Lian-Tao Wang,[3,4,§] and Xiao-Ping Wang[5,6,*]

[1]School of Physics and State Key Laboratory of Nuclear Physics and Technology, Peking University, Beijing 100871, China
[2]Center for High Energy Physics, Peking University, Beijing 100871, China
[3]Enrico Fermi Institute and Department of Physics, The University of Chicago, Chicago, Illinois 60637, USA
[4]Kavli Institute for Cosmological Physics, The University of Chicago, Chicago, Illinois 60637, USA
[5]School of Physics, Beihang University, Beijing 100083, China
[6]Beijing Key Laboratory of Advanced Nuclear Materials and Physics, Beihang University, Beijing 100191, China

(Received 25 October 2022; accepted 18 April 2023; published 11 May 2023)

Models with an axionlike particle (ALP) can provide an explanation for the discrepancy between experimental measurement of the muon anomalous-magnetic moment $(g-2)_\mu$ and the Standard Model prediction. This explanation relies on the couplings of the ALP to the muon and the photon. We also include more general couplings to the electroweak gauge bosons and incorporate them in the calculations up to the 2-loop order. We investigate the existing experimental constraints and find that they do not rule out the ALP model under consideration as a possible explanation for the $(g-2)_\mu$ anomaly. At the same time, we find the future Tera-Z and Higgs factories, such as the CEPC and FCC-ee, can completely cover the relevant parameter space through searches with final states $(\gamma\gamma)\gamma$, $(\mu^+\mu^-)\gamma$, and $(\mu^+\mu^-)\mu^+\mu^-$.

DOI: 10.1103/PhysRevD.107.095016

I. INTRODUCTION

The strong CP problem in the Standard Model (SM) [1–4] can be solved by the Peccei-Quinn mechanism, leading to the prediction of the existence a pseudo-Nambu-Goldstone boson, the axion [5–9]. The shift symmetry of the axion implies that it only has derivative couplings except for nonperturbative effects through strong interactions. In addition, other axionlike particles (ALPs) are ubiquitous in many new physics scenarios. Similar to the QCD axion, an ALP is a pseudo-Goldstone boson with an approximate shift symmetry. The corresponding decay constant f_a and mass m_a can be free parameters. It shares similar interactions with the QCD axion at low energy and predicts a rich phenomenology to be explored in various experiments [10–16].

The anomalous magnetic-dipole moment of the muon, $(g-2)_\mu$ is a powerful tool to test the SM and probe the physics beyond the Standard Model [17–21]. The combined results of the measurements at the Brookhaven National Laboratory [22] and the Fermi National Accelerator Laboratory [23] suggest a 4.2σ discrepancy between the SM prediction [24–44] and experiment measurement, as $\Delta a_\mu \equiv a_\mu^{\mathrm{Exp}} - a_\mu^{\mathrm{SM}} = (25.1 \pm 5.9) \times 10^{-10}$. It is worth noting that the status of the theoretical calculation of the SM prediction has not been settled yet [45,46]. In this paper, we make the assumption that the apparent discrepancy is due to the contribution of new physics beyond the Standard Model.

In this work, we focus on a scenario with the contribution of an ALP as the explanation of the apparent deviation in $(g-2)_\mu$. Since the ALP is a pseudoscalar, the axion-muon coupling contributes Δa_μ negatively. Therefore, a model in which this is the dominant coupling can not explain the $(g-2)_\mu$ anomaly. If the axion-photon coupling have a different sign comparing with the axion-muon coupling, the contribution can be positive [15,47–55]. Therefore, both of these couplings need to be present at the same time. Since the axion-photon coupling comes from the interaction with

†jialiu@pku.edu.cn
‡themapku@stu.pku.edu.cn
§liantaow@uchicago.edu
*Corresponding author.
hcwangxiaoping@buaa.edu.cn

hypercharge gauge field and $SU(2)_L$ gauge fields, in general, we should include both of them in addition to the muon coupling. Taking into account these considerations, we have the following effective Lagrangian at weak-scale energy

$$\mathcal{L}_{\text{eff}}^{\text{D}\leq 5} = \sum_f \frac{C_{ff}}{2}\frac{\partial^\mu a}{f_a}\bar{f}\gamma_\mu\gamma_5 f + \frac{g^2}{16\pi^2}C_{WW}\frac{a}{f_a}W^i_{\mu\nu}\tilde{W}^{\mu\nu,i} + \frac{g'^2}{16\pi^2}C_{BB}\frac{a}{f_a}B_{\mu\nu}\tilde{B}^{\mu\nu}, \quad (1)$$

where W and B are the $SU(2)_L$ and $U(1)_Y$ field strength. In this paper, we study the existing constraints on the parameters in Eq. (1) from collider searches, and propose to exploit searches with final states $(\gamma\gamma)\gamma$, $(\mu^+\mu^-)\gamma$, and $(\mu^+\mu^-)\mu^+\mu^-$ at future electron-positron colliders [56,57], with runnings in both the Tera-Z and the Higgs factory modes, to search for the ALP. We found that future Z factories can cover most of the parameter region of m_a up to 85 GeV, which can explain the $(g-2)_\mu$ anomaly, while future Higgs factories can extend the limits to much higher masses.

The $(g-2)_\mu$ and the constraints on the axion couplings have been extensively studied in Refs. [15,51,53–55]. Our work extends these results in the following aspects.

The 2-loop Barr-Zee diagram contributing to the $(g-2)_\mu$ has a nontrivial counterterm arising from the axion shift symmetry in the derivative coupling basis, which is clarified recently in Ref. [54]. Their calculations only consider the photon in the diagram. In our study, since we are interested in axion mass up to Z mass, the contributions from the W/Z gauge boson are also included.

Previous studies on the constraints from other experimental searches focus on the effect of turning on a single coupling. We start with both the fermion coupling $C_{\mu\mu}$ and the gauge boson coupling C_{BB} and C_{WW} due to the requirement of $(g-2)_\mu$. It opens up some unique channels, for example $Z \to (\mu^+\mu^-)\gamma$, in the multiple-parameters scenario. It differs from a previous study of $Z \to (\mu^+\mu^-)\gamma$ in Ref. [51], which only focused on $C_{\mu\mu}$ and derived $C_{\gamma Z}$ from the lepton coupling at the 1-loop level. Therefore, we conducted a reanalysis of this channel in the context of multiple parameters and particularly focused on its implications for the $(g-2)_\mu$ parameter region at future electron-positron colliders. In addition, we update the constraints from various existing experiments. For example, the muonic force study on $U(1)_{L_\mu - L_\tau}$ at the CMS [58] can set limits on the axion-muon coupling, but it is missing in the previous studies. Moreover, with two gauge couplings, one of the couplings $C_{\gamma\gamma}$ or $C_{Z\gamma}$ can be very small, leading to significant changes in the axion-decay branching ratio and lifetime. Therefore, some previous studies do not directly apply to this case.

We should also mention the flavor physics measurements can, in principle, offer sensitive probes to axion couplings. For instance, in a UV completion of the ALP Lagrangian, there may exist flavor off-diagonal derivative couplings between the ALP and leptons. Such couplings could trigger charged-lepton flavor-violation processes such as $\mu \to e\gamma$ and $\pi \to \mu e$ and are consequently stringently constrained by experimental results [52,53,55,59]. Hence, we assume that the ALP-lepton coupling is flavor diagonal at low-energy scales in the lepton-mass basis. This setting implies that the UV completion of the ALP model must possess a specific flavor structure to account for the pronounced suppression of flavor off-diagonal couplings [54,55]. Furthermore, the C_{WW} coupling can induce the flavor-violating couplings in the down-quark sector through the top quark in the loop, which is severely constrained by the precision meson measurements. The C_{WW} coupling can be constrained by $B^+ \to K^+ a(\mu\mu)$, $B \to K^* a(\mu\mu)$, $B^+ \to \pi^+ a(\mu\mu)$ for $m_a < 5$ GeV [55]. The C_{BB} coupling is less constrained since it comes in at a higher order. For $C_{\mu\mu}$ coupling, the three exotic B meson decay channels provide similar constraints. There is one more channel $B_s \to \mu^+\mu^-$, which can provide a constraint competitive with the CMS-muonic force search [58] even for large m_a. At the same, such constraints depend on the flavor model, which necessarily involves more parameters. In this paper, we will assume that flavor constraints are not enough to cover the interesting parameter space.

The paper is organized as follows. In Sec. II, we describe the axion low-energy model and calculate the $(g-2)_\mu$ at the 2-loop level. In Sec. III, we start without the coupling between the ALP and the W boson. The signal final states are classified as $a+\gamma$ and $a+\bar{f}f$ and the existing constraints from electron-positron colliders like *BABAR* [60,61], Belle-II [62], the LEP [63–66], and the Large Hadron Collider [58,67,68] are discussed extensively in Sec. III A. We then discuss the constraints from exotic final states at future Tera-Z and Higgs factory in Sec. III B and extend the results including the general couplings to W boson in Sec. III D. Section IV contains our conclusion.

II. THE ALP PROPERTIES AND CONTRIBUTION TO $(g-2)_\mu$

In this section, we present analytical results useful for our numerical study, including the ALP couplings, relevant decay widths, and their contribution to $(g-2)_\mu$. Following the notation of [54], we begin with the effective Lagrangian on the basis of the fermion masses.

$$\mathcal{L}_{\text{eff}}^{\text{D}\leq 5} = \sum_f \frac{C_{ff}}{2}\frac{\partial^\mu a}{f_a}\bar{f}\gamma_\mu\gamma_5 f + \frac{\alpha C_{\gamma\gamma}}{4\pi}\frac{a}{f_a}F_{\mu\nu}\tilde{F}^{\mu\nu} + \frac{\alpha C_{\gamma Z}}{2\pi s_w c_w}\frac{a}{f_a}F_{\mu\nu}\tilde{Z}^{\mu\nu} + \frac{\alpha C_{ZZ}}{4\pi s_w^2 c_w^2}\frac{a}{f_a}Z_{\mu\nu}\tilde{Z}^{\mu\nu} + \frac{\alpha C_{WW}}{\pi s_w^2}\frac{a}{f_a}\epsilon_{\mu\nu\rho\sigma}\partial^\mu W_+^\nu \partial^\rho W_-^\sigma + \cdots, \quad (2)$$

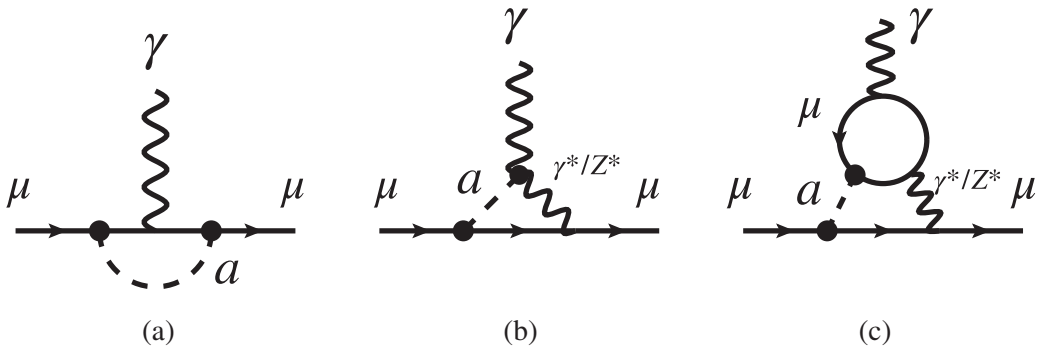

FIG. 1. The loop diagrams with ALP for $(g-2)_\mu$ up to 2-loop level. The gauge bosons in diagrams (b) and (c) are γ and Z bosons.

with the coefficients

$$C_{\gamma\gamma} = C_{WW} + C_{BB}, \qquad C_{\gamma Z} = c_w^2 C_{WW} - s_w^2 C_{BB},$$
$$C_{ZZ} = c_w^4 C_{WW} + s_w^4 C_{BB}, \tag{3}$$

where $s_w \equiv \sin\theta_W$, $c_w \equiv \cos\theta_W$ with θ_W being the weak-mixing angle. This EFT Lagrangian can be valid up to scale $\Lambda = 4\pi f_a$ [54,55]. We have omitted the gluon coupling and interaction vertices containing more than three fields. In this work, we only consider $f = \mu$ for simplicity.

For illustrative purposes, we start with a simple case $C_{WW} = 0$ to present our analytic results and discuss experimental constraints before we present the full numerical results with $C_{WW} \neq 0$. This simple choice is also favored by electroweak precision data (EWPD) (see, e.g., Fig. 27 of Ref. [15]). In this case, we have three free parameters

$$\{m_a, C_{\mu\mu}, C_{BB}\}. \tag{4}$$

In this case, the exotic Z decay $Z \to \gamma a$ is induced by $C_{Z\gamma} = -s_w^2 C_{BB} = -s_w^2 C_{\gamma\gamma}$. The partial widths of the exotic Z decay and the two axion decay channels $a \to \mu^+\mu^-$ and $a \to \gamma\gamma$ are

$$\Gamma(Z \to \gamma a) = \frac{\alpha^2(m_Z) m_Z^3}{96\pi^3 s_w^2 c_w^2 f_a^2} |C_{\gamma Z}^{\rm eff}|^2 \left(1 - \frac{m_a^2}{m_Z^2}\right)^3, \tag{5}$$

$$\Gamma(a \to \mu^+\mu^-) = \frac{m_a m_\mu^2}{8\pi f_a^2} |C_{\mu\mu}^{\rm eff}|^2 \sqrt{1 - \frac{4m_\mu^2}{m_a^2}}, \tag{6}$$

$$\Gamma(a \to \gamma\gamma) = \frac{\alpha^2 m_a^3}{64\pi^3 f_a^2} |C_{\gamma\gamma}^{\rm eff}|^2, \tag{7}$$

where the effective couplings are

$$C_{\gamma\gamma}^{\rm eff} = C_{\gamma\gamma} + C_{\mu\mu}\left[1 + \frac{m_\mu^2}{m_a^2} \cdot \mathcal{F}\left(\frac{m_a^2}{m_\mu^2}\right)\right] + \mathcal{O}(\alpha), \tag{8}$$

$$C_{\gamma Z}^{\rm eff} = C_{\gamma Z} + C_{\mu\mu}\left(\frac{1}{4} - s_w^2\right)\left[1 + \frac{m_\mu^2}{m_a^2 - m_Z^2} \cdot \left(\mathcal{F}\left(\frac{m_a^2}{m_\mu^2}\right) - \mathcal{F}\left(\frac{m_Z^2}{m_\mu^2}\right)\right)\right] + \mathcal{O}(\alpha), \tag{9}$$

$$C_{\mu\mu}^{\rm eff} = C_{\mu\mu} + \mathcal{O}(\alpha^2), \tag{10}$$

$$\mathcal{F}(x) \equiv \ln^2\left(\frac{\sqrt{x(x-4)} - x + 2}{2}\right), \tag{11}$$

with the fine-structure constant evaluated at Z-pole $\alpha(m_Z) \approx 1/127.9$. Since the axion gauge-boson coupling $C_{\gamma\gamma}, C_{\gamma Z}$ enters to the $(g-2)_\mu$ at 1-loop, it is necessary to include the 1-loop contributions in the effective couplings. The effective couplings presented here are consistent with those in Ref. [15].

A. The contribution to the $(g-2)_\mu$

In this leptophilic-axion setup, there are three types of diagrams, shown in Fig. 1, contributing to the $(g-2)_\mu$ and potentially giving an explanation to Δa_μ [54]. The first two are 1-loop diagrams from muon and photon/Z boson couplings, and the third one is the Barr-Zee-type diagram from muon coupling only. The first diagram $a_\mu^{(1)}$ and third diagram $a_\mu^{(3)}$ contribute negatively to Δa_μ, with $a_\mu^{(1,3)} \propto -C_{\mu\mu}^2$. This can be understood by the fact that the axion is CP-odd pseudoscalar, resulting in an extra minus sign in comparison with the scalar. Therefore, to explain the $(g-2)_\mu$ anomaly, the contribution of the second diagram $a_\mu^{(2)} \propto -C_{\mu\mu} C_{\gamma\gamma}$ has to be positive, implying that the couplings $C_{\mu\mu}$ and $C_{\gamma\gamma}$ should have different sign [15,47,50]. Without loss of generality, from now on, we assume that $C_{\gamma\gamma}/C_{BB}$ is positive while $C_{\mu\mu}$ is negative.

The contributions of the diagrams in Fig. 1 are given by

$$\Delta a_1 = -\frac{C_{\mu\mu}^2 m_\mu^2}{16\pi^2 f_a^2}\left[1+2x+x(1-x)\ln(x) + \frac{2x(x-3)}{x-4}\sqrt{x(x-4)}\ln\left(\frac{\sqrt{x-4}+\sqrt{x}}{2}\right)\right], \quad (12)$$

$$\Delta a_{2\gamma} = -\frac{\alpha m_\mu^2 C_{\mu\mu} C_{\gamma\gamma}}{8\pi^3 f_a^2}\cdot h_\gamma(x,\Lambda), \quad (13)$$

$$\Delta a_{2Z} = \frac{\alpha C_{\gamma Z} C_{\mu\mu} m_\mu^2 (4s_w^2-1)}{32\pi^3 c_w^2 s_w^2 f_a^2}\cdot h_Z(x,y,\Lambda), \quad (14)$$

$$\Delta a_{3\gamma} = -\frac{\alpha C_{\mu\mu} C_{ff}}{8\pi^3}\frac{m_\mu^2}{f_a^2}[H_\gamma + h_\gamma(x,\Lambda)], \quad (15)$$

$$\Delta a_{3Z} = -\frac{\alpha C_{\mu\mu} C_{ff} m_\mu^2 (4s_w^2-1)^2}{128\pi^3 c_w^2 s_w^2 f_a^2}[H_Z + h_Z(x,y,\Lambda)], \quad (16)$$

where the $H_{\gamma/Z}$ and $h_{\gamma/Z}$ functions are

$$H_Z = \int_0^1 dz\left\{\frac{\Delta^2}{\Delta^2-m_a^2}\left[-\frac{m_a^2(m_a^2+2m_\mu^2)B(m_\mu^2,m_a,m_\mu)}{3(m_a^2-m_Z^2)m_\mu^2} + \frac{m_a^6}{6m_\mu^4(m_a^2-m_Z^2)}\ln\left(\frac{m_a^2}{m_\mu^2}\right)\right] + \frac{\Delta^2}{\Delta^2-m_Z^2}\left[\frac{m_Z^2(2m_\mu^2+m_Z^2)B(m_\mu^2,m_Z,m_\mu)}{3m_\mu^2(m_a^2-m_Z^2)} + \frac{m_Z^6}{6m_\mu^4(m_Z^2-m_a^2)}\ln\left(\frac{m_Z^2}{m_\mu^2}\right)\right] + \frac{\Delta^2}{3m_\mu^2} + \frac{\Delta^4(\Delta^2+2m_\mu^2)B(m_\mu^2,m_\mu,\Delta)}{3m_\mu^2(\Delta^2-m_a^2)(\Delta^2-m_Z^2)} + \frac{\Delta^8}{6m_\mu^4(\Delta^2-m_a^2)(\Delta^2-m_Z^2)}\ln\left(\frac{m_\mu^2}{\Delta^2}\right)\right\}, \quad (17)$$

$$H_\gamma = \int_0^1 dz\frac{\Delta^2}{2(\Delta^2-m_a^2)}\left[-\frac{2}{3}\frac{m_a^2+2m_\mu^2}{m_\mu^2}B(m_\mu^2,m_a,m_\mu) + \frac{2}{3}\frac{\Delta^2+2m_\mu^2}{m_\mu^2}B(m_\mu^2,m_\mu,\Delta) + \frac{\Delta^4}{3m_\mu^4}\ln\left(\frac{m_\mu^2}{\Delta^2}\right) + \frac{m_a^4}{3m_\mu^4}\ln\left(\frac{m_a^2}{m_\mu^2}\right) + \frac{2}{3}\frac{\Delta^2-m_a^2}{m_\mu^2}\right]. \quad (18)$$

$$h_\gamma = \ln\left(\frac{\Lambda^2}{m_\mu^2}\right) + 2 - \frac{x^2}{6}\ln(x) + \frac{x}{3} + \frac{x+2}{3}\sqrt{x(x-4)}\ln\left(\frac{\sqrt{x-4}+\sqrt{x}}{2}\right), \quad (19)$$

$$h_Z = \ln\left(\frac{\Lambda^2}{m_Z^2}\right) + \frac{x(x+2)B(m_\mu^2,m_a,m_\mu)}{3(x-y)} + \frac{y(2+y)B(m_\mu^2,m_Z,m_\mu)}{3(y-x)} + \frac{(x+6+y)}{3} - \frac{6x+y^3-6y}{6(x-y)}\ln\left(\frac{x}{y}\right) - \frac{x^2+xy-6+y^2}{6}\ln(x), \quad (20)$$

with

$$x \equiv \frac{m_a^2}{m_\mu^2}, \qquad y \equiv \frac{m_Z^2}{m_\mu^2}, \qquad \Delta^2 \equiv \frac{m_f^2}{z(1-z)}, \quad (21)$$

$$B(m_\mu^2, m_{a/Z}, m_\mu) = \sqrt{m_{a/Z}^2(m_{a/Z}^2-4m_\mu^2)}\ln\left(\frac{\sqrt{m_{a/Z}^2-4m_\mu^2}+m_{a/Z}}{2m_\mu}\right)/m_\mu^2, \quad (22)$$

$$B(m_\mu^2, m_\mu, \Delta) = \sqrt{\Delta^2(\Delta^2-4m_\mu^2)}\ln\left(\frac{\sqrt{\Delta^2-4m_\mu^2}+\Delta}{2m_\mu}\right)/m_\mu^2. \quad (23)$$

The B function is the **DiscB** function in Mathematica Package X [69]. Λ is the loop calculation UV cutoff scale. In our muonphilic scenario, the loop fermion is restricted to the muon lepton only, i.e., $f=\mu$. Explicit calculations have been performed in Refs. [15,50,54], with the inner loop of the Barr-Zee diagram using off shell axion and photon propagators when connecting to the muon lines [54]. The effective $aF\tilde{F}$ vertex function is then inserted into the loop, which leads to the final answer of $(g-2)_\mu$. As an appropriate approximation, we only keep effective vertex function result that is linear in the on shell photon's momentum.

In addition, we add the contribution with internal Z boson for completeness, denoted as Δa_{2Z} and Δa_{3Z}, especially because we are interested in large m_a comparable to m_Z. Moreover, for nonzero C_{WW}, it is possible that $C_{\gamma Z}$ can be much larger than $C_{\gamma\gamma}$. Thus the diagram with Z boson in the loop is no longer negligible. The result in the second diagram of Fig. 1 with an inner Z boson takes the form $\Delta a_{2Z} \propto \log\frac{\Lambda^2}{m_Z^2}+3/2$ when expanded at large y, which is consistent with calculations of Ref. [15]. In the third diagram of Fig. 1, the contribution with internal Z boson to the Barr-Zee diagram is not small due to the counter-term (explained in detail below). Lastly, due to the ALP's antisymmetric coupling to the $W^\pm$ gauge bosons, the contribution of the 2-loop Barr-Zee diagram with the W boson in the loop is zero [55,70].

The calculations in Eqs. (12)–(16) are done with shift-invariant derivative coupling $\partial^\mu a\bar{f}\gamma_\mu\gamma_5 f$, which has a subtlety in the last diagram. A direct 2-loop calculation of the third diagram leads to the H function. However, the vertex function of the inner loop is ambiguous since it is linearly divergent. For the inner loop leading to an effective $aF\tilde{F}$ vertex, it has to vanish when sending the fermion mass in the inner loop to infinity to preserve the shift symmetry of ALP. This fact is not satisfied for H function alone. Therefore, one has to add the counterterm function h to fix this problem as shown in Ref. [54]. The counterterm here works as a shift-symmetry restoration in the derivative coupling basis and should not be mixed with the counterterms in renormalization procedure.

It turns out that the function h dominates over H in the parameter space we are interested in. It is suggestive to compare with the results in the other operator basis. One can do a chiral rotation to eliminate the derivative term, which is equivalent to doing the following substitution,

$$\begin{aligned}&\frac{C_{ff}}{2}\frac{\partial^\mu a}{f_a}\bar{f}\gamma_\mu\gamma_5 f\\&\quad\to -\frac{C_{ff}m_f}{f_a}a\bar{f}i\gamma_5 f+\frac{g'^2(Y_L^2+Y_R^2)C_{ff}}{32\pi^2 f_a}aB^{\mu\nu}\tilde{B}_{\mu\nu}\\&\qquad+\frac{g^2T_3^2C_{ff}}{32\pi^2 f_a}aW_{3\mu\nu}\tilde{W}_3^{\mu\nu}+\frac{gg'T_3Y_LC_{ff}}{16\pi^2 f_a}aB_{\mu\nu}\tilde{W}_3^{\mu\nu}+\cdots\end{aligned}\tag{24}$$

$$\begin{aligned}&\to -\frac{C_{ff}m_f}{f_a}a\bar{f}i\gamma_5 f+\frac{\alpha Q^2C_{ff}}{4\pi f_a}aF_{\mu\nu}\tilde{F}^{\mu\nu}\\&\quad+\frac{\alpha C_{ff}Q(\frac{1}{2}T_3-s_w^2Q)}{2\pi c_w s_w f_a}aF^{\mu\nu}\tilde{Z}_{\mu\nu}\\&\quad+\frac{\alpha C_{ff}(s_w^4Q^2-s_w^2QT_3+\frac{T_3^2}{2})}{4\pi c_w^2 s_w^2 f_a}aZ^{\mu\nu}\tilde{Z}_{\mu\nu}+\cdots,\end{aligned}\tag{25}$$

where Y_L, Y_R, and T_3 are the hypercharge of left-handed, right-handed, and weak isospin of fermions, respectively. We have omitted the terms which are higher order in f_a^{-1}. The anomalous $aF^{\mu\nu}\tilde{Z}_{\mu\nu}$ part can be determined by the calculation of anomalous triangle diagrams with massless fermions running in the loop. Because of the Furry theorem, only the vector part of Z coupling to fermions contributes to the diagrams. When using the $ia\bar{\mu}\gamma_5\mu$ operator, the result for the first diagram is not changed, while the third diagram returns exactly the H function. Since there is no shift symmetry, the results are exact. Furthermore, the extra $aF^{\mu\nu}\tilde{F}_{\mu\nu}$ coupling in Eq. (25) leads to a new contribution in the second diagram, which matches the counterterm contribution as the h function. We have done the calculation using Package-X [69]. The results of the H functions are consistent with other calculations. For the 2-loop calculations, when the loop fermion mass m_f and the ALP mass m_a satisfy the condition ($m_\mu \ll m_a, m_f$), our results of the H functions coincide with the 2-loop results in Ref. [47] calculated with $i\bar{\mu}\gamma_5\mu$.

In Fig. 2, using Eqs. (12)–(16), we show the parameter space which can give an explanation to the $(g-2)_\mu$ anomaly at 2σ confidence level. The axion mass is chosen to be 1, 5, 10, 50, 70, 80, and 100 GeV, respectively, which will also serve as benchmark cases for the rest of the paper. In the shaded regions between different color lines, an explanation of the $(g-2)_\mu$ anomaly is possible. In these regions, the decay to dimuon dominates over the diphoton except at high-mass regions around Z-pole. For the upper-right region, the $C_{\mu\mu}$ coupling is large and leads to a large negative contribution, which requires a large $C_{\gamma\gamma}$ coupling to cancel it. For larger couplings, this cancellation needs to be more precise. Hence, there is less flexibility for $C_{\gamma\gamma}$, and the band on the upper-right region is much thinner than the upper-left region.

The results presented in Fig. 2 indicate that a minimum value of $\frac{C_{\gamma\gamma}}{f_a}$ can be around 40 TeV^{-1} to explain the $(g-2)_\mu$ anomaly. This implies that the EFT Lagrangian given in Eq. (2) should be valid up to the cutoff $\Lambda = 4\pi f_a \sim$ 300 GeV, which in turn suggests that $f_a \ll v_{\rm SM}$, with $v_{\rm SM}=246$ GeV being the SM electroweak-breaking scale. Consequently, the applicability of the EFT to the underlying UV model is a challenge, and the constraints on the UV complete model may be important in phenomenological constraints on EFT. These challenges have been

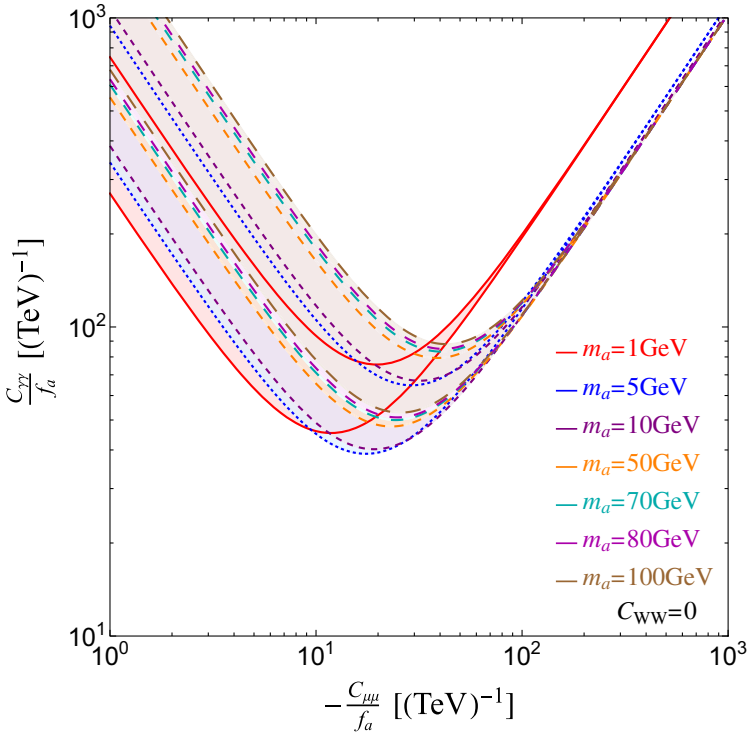

FIG. 2. The bands in the axion couplings which can give an explanation to the $(g-2)_\mu$ anomaly at 2σ confidence level. Different bands correspond to different choices of axion mass m_a. We set the cutoff scale, Λ, to be 1 TeV and the axion-W coupling $C_{WW}=0$.

comprehensively discussed in Ref. [54], which notes that the flavor off-diagonal derivative coupling of the ALP is inevitable, and therefore lepton flavor-violating processes should be considered. We take all relevant points into account, as recommended in Ref. [54]. Our findings suggest that there is still room for ALP $(g-2)_\mu$ explanation, which could be explored in future collider searches.

III. THE CONSTRAINTS FROM EXISTING SEARCHES AND PROJECTION OF FUTURE PROBES

The model of ALP with an explanation for the $(g-2)_\mu$ anomaly can lead to a rich set of experimental signals. For example, there are many existing experiments searching for light new particles in a similar mass range, which can set stringent limits on ALP couplings. In Sec. III A, we will go through the existing experiments and check how they can constrain the above parameter space. It turns out that most of the interesting parameter space capable of explaining the $(g-2)_\mu$ anomaly is still viable under the existing constraints.

In addition, the above couplings can lead to exotic Z decay $Z\to a\gamma$ and $Z\to a\mu^+\mu^-$, as shown in Fig. 3, with relevant branching ratios presented in Fig. 4. These are the main decay channels we will be considering in this paper. We discuss the limits from the Z-pole run at future electron-positron colliders in Sec. III B and found it can decisively exclude the ALP solution up to $m_a\sim 85$ GeV. In this section, we will focus on the simpler case of $C_{WW}=0$. This gives a simple picture of physics. In Sec. III D, we will present the numerical results with nonzero C_{WW} and discuss the difference with the simpler case.

A. Constraints from current results of light-particle searches

We focus on two final states, one is $a+\gamma$ and the other is $a+\bar{f}f$. In addition, axion decay channels, $a\to\gamma\gamma$ and $a\to\mu^+\mu^-$, are considered. In the following, we will go through the relevant experiments and set the limits on the ALP couplings to muon and photon.

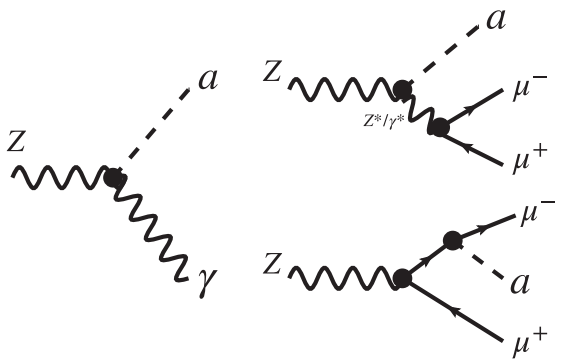

FIG. 3. The Feynman diagrams for exotic Z decay channels $Z\to a\gamma$ and $Z\to a\mu^+\mu^-$, respectively.

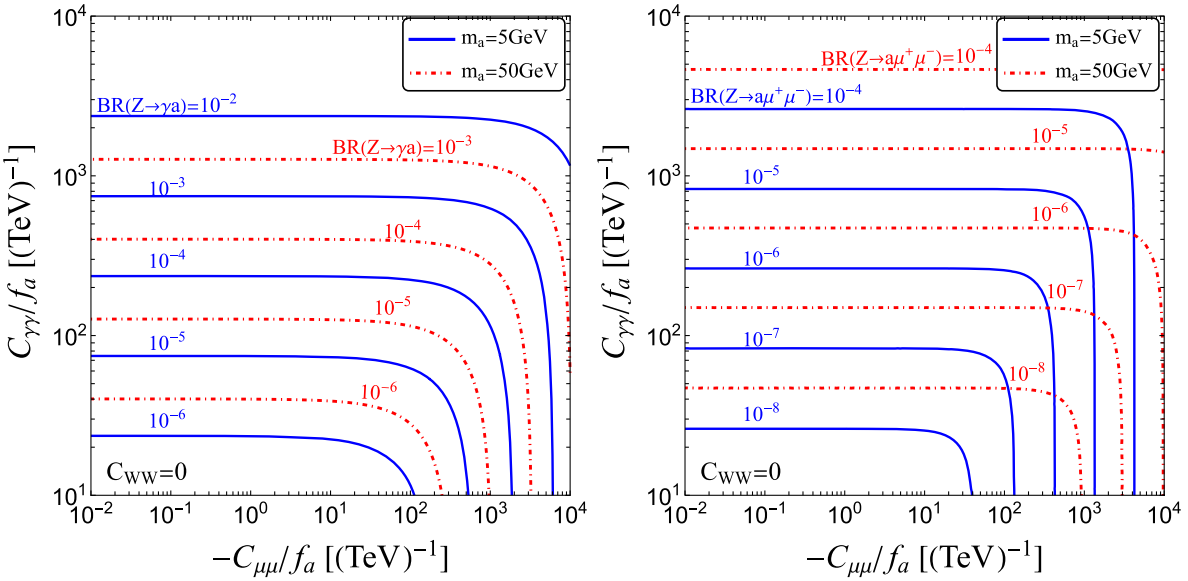

FIG. 4. The exotic Z decay branching ratios for $Z \to a\gamma$ (left panel) and $Z \to a\mu^+\mu^-$ (right panel), respectively. As examples, we choose $C_{WW} = 0, m_a = 5$ GeV and 50 GeV.

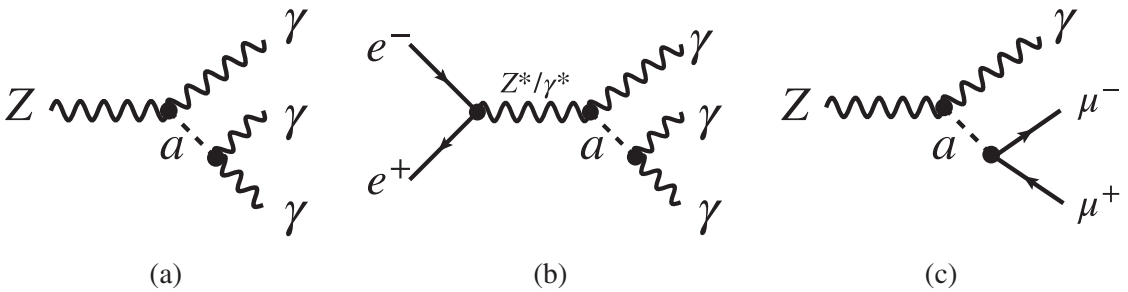

FIG. 5. Feynman diagrams corresponding to $a + \gamma$ final states in various experimental searches. The diagram (a) is related to LEP/L3/ATLAS [65–67] with on shell $Z \to (\gamma\gamma)\gamma$, while diagrams (b) and (c) are related to OPAL searches for $e^+e^- \to (\gamma\gamma)\gamma$ via off shell γ/Z [63] and on shell $Z \to (\mu^+\mu^-)\gamma$ [64], respectively.

1. Constraints from searches for final states of $a+\gamma$

An ALP together with a photon can show up as final states from either exotic Z decay $Z \to a\gamma$ or the s-channel off shell photons and Z bosons production $e^+e^- \to \gamma^*/Z^* \to a\gamma$, though couplings $C_{\gamma\gamma}$ and $C_{\gamma Z}$ (for $C_{WW} = 0$, $C_{\gamma Z}$ is fixed by $C_{\gamma\gamma}$) as shown in Fig. 5. Since both $C_{\mu\mu}$ and $C_{\gamma\gamma}$ are nonzero in order to account for the $(g-2)_\mu$ anomaly, the ALP will decay to $\mu^+\mu^-$ and $\gamma\gamma$. Therefore, the experimental searches for $(\gamma\gamma)+\gamma$ and $(\mu^+\mu^-)+\gamma$ final states, where the bracket indicates the two particles inside form a resonance, should be sensitive to this class of models.

(i) *Two photon final state $\gamma\gamma$*: There have been a large number of relevant searches at LEP and LHC which focus on multiphoton final state. For very low-mass ALPs, the two photons decayed from boosted ALPs are too collimated to be resolved by the detector. Therefore, the two photons will be recognized as one single photon. As a result, in the low mass region the 2γ final-state search is more relevant. LEP-I inclusive diphoton searches $e^+e^- \to X + 2\gamma$ is exploited to cover the low-mass ALPs in Refs. [65,71]. The Z-pole production $Z \to a\gamma$ and virtual photon production $e^+e^- \to \gamma^*/Z^* \to a\gamma$ have been considered and the limits on $C_{\gamma Z}$ and $C_{\gamma\gamma}$ have been derived with the assumption $\mathrm{BR}(a \to \gamma\gamma) = 100\%$. With the inclusion of $a \to \mu^+\mu^-$, it can still place the most stringent bound for $m_a = 1$ GeV as shown in Fig. 8 and for $m_a < 4$ GeV as shown in the right panel of Fig. 9.

(ii) *Three photon final state $(\gamma\gamma)\gamma$ where the pair $(\gamma\gamma)$ come from the ALP decay*[1]: The searches based on this final state are relevant for higher ALP masses. L3 and ATLAS have looked for exotic Z decay $Z \to 3\gamma$ [66,67], while the OPAL Collaboration has searched for off shell γ/Z process $e^+e^- \to X(\gamma\gamma)\gamma$

[1]In this paper, we use the convention that two particles inside a bracket come from the ALP.

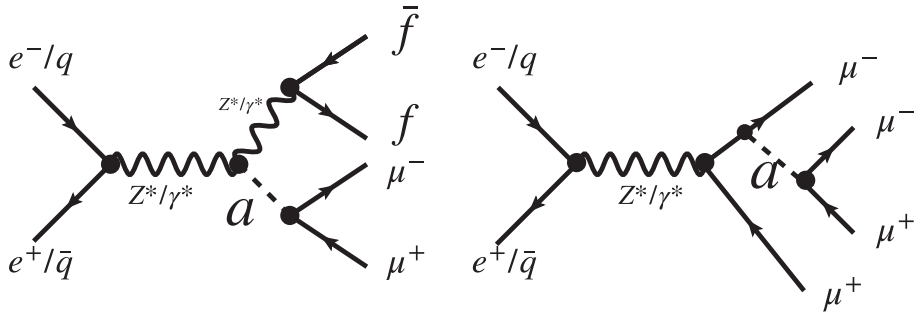

FIG. 6. Feynman diagrams corresponding to $a + f\bar{f}$ final states experiments searches. Diagram (a) is related to the collider searches $e^+e^-/pp \to (\mu^+\mu^-)f\bar{f}$ at *BABAR* [60,61], CMS [58,68], and diagram (b) is also related to the collider searches $e^+e^-/pp \to (\mu^+\mu^-)\mu^+\mu^-$ at CMS [58], *BABAR* [61].

[63]. The ATLAS experiment sets a limit $\mathrm{BR}(Z \to \gamma\gamma\gamma) < 2.2 \times 10^{-6}$ [67], which can be used to put constraints on $M_a \lesssim 70$ GeV. There is no limit on $m_a > 70$ GeV due to the experimental requirement $p_T^\gamma > 17$ GeV [72]. Recently, Belle-II has searched for the channel $e^+e^- \to \gamma a \to 3\gamma$ at electron-positron colliders for ALP mass range $0.2 < m_a < 9.7$ GeV [62], assuming $\mathrm{BR}(a \to \gamma\gamma) = 100\%$. After including the ALP-decay branching ratio to muons, these experiment results can be recast to set stringent limits on axion-photon coupling $C_{\gamma\gamma}$. In the right panel of Fig. 9, we have assumed that for a given $C_{\gamma\gamma}$ and m_a, the coupling to muon $C_{\mu\mu}$ is the minimal value which can give an explanation to the $(g-2)_\mu$ anomaly. In this case, one can see the limits on $C_{\gamma\gamma}/f_a$ should be $\lesssim 300$ TeV^{-1} by LEP-I (2γ) for $m_a < 10$ GeV and $\lesssim 100$ TeV^{-1} by L3 3γ for 4 GeV $< m_a < m_Z$. The ATLAS $(Z \to 3\gamma)$ search is a little stronger than L3 $(Z \to 3\gamma)$, but is narrower in the mass range covered. OPAL (3γ) can set limits on $C_{\gamma\gamma}/f_a < \mathcal{O}(150)$ TeV^{-1} for $m_a > 20$ GeV and can extend to limit to $m_a \lesssim 190$ GeV [71].

(iii) *Muon pair with a radiated photon* $(\mu^+\mu^-) + \gamma$: If ALP decays to muons, the experimental search for final state $\mu^+\mu^-\gamma$ is relevant. The OPAL Collaboration has studied a pair of leptons $\ell^+\ell^-$ plus a radiated photon from a Z decay [64], where $\ell = e$, μ, τ, and set limits on the exotic Z decay $\mathrm{Br}(Z \to \mu^+\mu^-\gamma) < 5.6 \times 10^{-4}$. They have also set limits for new resonance from $Z \to X\gamma$ with $X \to \ell^+\ell^-$ for 60 GeV $< m_X <$ 84 GeV. It has been used to constrain $C_{Z\gamma}$ while assuming axion decay $\mathrm{Br}(a \to \ell^+\ell^-) = 100(10)\%$ in Ref. [15]. We adapt the results to our model with both $C_{\gamma\gamma}$ and $C_{\mu\mu}$ couplings. However, with the choice $C_{WW} = 0$, it only shows up in the left panel in Fig. 9, where our choice of minimal $C_{\gamma\gamma}$ leads to larger $\mathrm{BR}(a \to \mu^+\mu^-)$. In the right panel of Fig. 9, this limit is not relevant and the constraints are dominated by the photon final state searches.

2. Constraints from searches for final states of $a + \bar{f}f$

The relevant processes with this class of final states are shown in Fig. 6. Depending on whether the fermion is muon lepton or not, this final state can be classified into two categories.

(i) *A muon pair together with a pair of other fermions* $(\mu^+\mu^-) + \bar{f}f$: If the associated fermions are not muons, the ALP should be generated through axion-gauge couplings alone as shown in the left panel of Fig. 6. In this case, to recast the experiment limits to our model, we need to rescale the constraint on axion-gauge couplings by taking into account the $a \to \mu^+\mu^-$ branching ratio.

Several experimental searches belong to this category. The CMS Collaboration has analyzed multilepton final states in search for new scalar or pseudoscalar particles, which decay to dimuon or dielectron, assuming the particle is produced in pp collisions associated with top-quark pairs, i.e., $pp \to t\bar{t}\phi$ with $\phi \to \mu^+\mu^-$ [68]. Recently, the *BABAR* Collaboration [60] has published a search result for dark leptophilic scalar in the channel $e^+e^- \to \tau^+\tau^-\phi_L, \phi_L \to \ell^+\ell^-$, setting limits to leptonic couplings for ϕ_L in the mass range $0.04 < m_{\phi_L} < 7.0$ GeV. The ALP in our model can play the role for ϕ/ϕ_L here, generated in associated with top- or tau-lepton pairs and subsequently decays to a pair of muons. Their results can be recast to constrain couplings $C_{\gamma\gamma}/C_{\gamma Z}$. The CMS and the *BABAR* experiments can constrain the $|C_{\mu\mu}/f_a| \lesssim 5000$ TeV^{-1} and 1000 TeV^{-1} respectively, as shown in the left panel of Fig. 9. For the parameter region capable of explaining the $(g-2)_\mu$ anomaly, the constraints from the

$(\mu^+\mu^-)+\bar{f}f$ final state searches are less stringent compared with 4μ final states search.

(ii) *Four muons final state* $(\mu^+\mu^-)+\mu^+\mu^-$: If the fermions associated with an ALP are muons, the ALPs are generated through the couplings $C_{\gamma\gamma}$, $C_{\gamma Z}$, and $C_{\mu\mu}$. We can not simply rescale the existing ALP coupling limit (usually assuming only one ALP coupling) since more Feynman diagrams are relevant, which could alter the cut efficiency for the signal model. Therefore, we use MadGraph5@NLO [73] and FeynRules [74] to simulate and recast the experimental bounds.

There are a number of experimental searches for the 4μ final states, often targeting some mediator of the so-called muonic dark force, such as the $Z'_{L_\mu-L_\tau}$ gauge boson. The *BABAR* Collaboration [61] has carried out the $e^+e^-\to 4\mu$ channel analysis using 514 fb^{-1} data, looking for exotic gauge boson Z' in mass range of 0.212–10 GeV. The CMS Collaboration [58] has performed a similar search for Z' in mass range 10–70 GeV at LHC. In these results, the production and decay of the Z's are both assumed to be governed by a single coupling to muon. To recast their limits, both the couplings of $C_{\mu\mu}$ and $C_{\gamma\gamma/\gamma Z}$ need to be considered due to the differences in relevant Feynman diagrams and the effect of ALP decay branching ratio. In addition, the different cut efficiencies between vector gauge bosons and pseudoscalar have been taken into account by simulation. In the left panel of Fig. 9, the 4μ final state search places the most stringent constraints on parameter spaces relevant for explaining the $(g-2)_\mu$ anomaly. It excludes $|C_{\mu\mu}/f_a|\geq\mathcal{O}(10)$ TeV^{-1}.

3. Constraints from measurements of Light-by-Light scattering

Light-by-light scattering $\gamma\gamma\to\gamma\gamma$ can occur in heavy-ion collisions and proton-proton collisions, which is shown in Fig. 7. This type of scattering can be used to probe ALPs through channel $\gamma\gamma\to a\to\gamma\gamma$. There are several experimental searches for ALPs using the same final state as the light-by-light scattering process. CMS [75] and ATLAS [76] have analyzed the data collected from ultraperipheral Pb-Pb collisions at $\sqrt{s_{NN}}=5.02$ TeV and set upper limits for $C_{\gamma\gamma}/f_a$ assuming BR$(a\to\gamma\gamma)=100\%$. Similarly, the LHC has carried out several searches for exclusive diphoton events in proton-proton collisions [77,78] and set limits for the higher mass of ALPs. These experiments and their limitations of ALPs have been extensively studied in Ref. [79] and we rescale the constraints by the ALP decay branching ratio. We have placed these limits in the Fig. 9 and are denoted as PbPb$(\gamma\gamma)$ and LHC$\gamma\gamma$F for Pb-Pb and pp collisions, respectively.

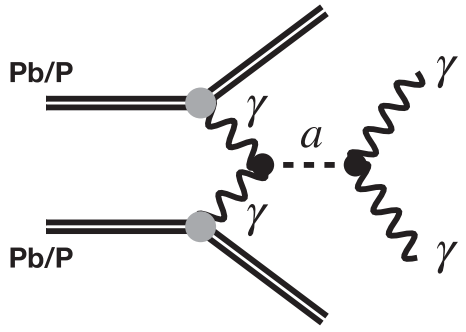

FIG. 7. The photon fusion process $\gamma\gamma\to a\to\gamma\gamma$ from Pb-Pb ion collision and pp collision at the LHC.

B. The search at future Z and Higgs factories

There have been several proposals for future circular electron-positron colliders, including the CEPC [56,80] and the FCC-ee [57,81]. As part of their proposed run plan, there is a stage running at the Z-pole with a target of resonant producing more than 10^{12} Z gauge bosons, as well as runs in the Higgs factory mode [56,82]. These are called Tera-Z and Higgs factories. In particular, FCC-ee (CEPC) is proposed to run an integrated luminosity at Z pole for 150 ab^{-1}(60 ab^{-1}) and at $\sqrt{s}=240$ GeV for 5 ab^{-1}(12 ab^{-1}), respectively [83,84]. With numerous Z and Higgs bosons and the clean environment of an electron-positron collider, it is an ideal place to look for the exotic Z and Higgs decay and place limits for beyond the Standard Model physics [71,85–90].

The couplings $C_{\gamma Z}$ and $C_{\mu\mu}$ are crucial for an ALP explanation of the $(g-2)_\mu$ anomaly. At the same time, they predict rare Z decays $Z\to a\gamma$ and $Z\to a\mu^+\mu^-$, which the Tera-Z factory is well-equipped to test. The axion decays dominantly via $a\to\mu^+\mu^-$ in the parameter space which can explain the $(g-2)_\mu$ anomaly, except when m_a is close to the Z-pole. In our numerical study, we have included the 1-loop correction from muon coupling $C_{\mu\mu}$ to the ALP couplings $C_{\gamma Z/\gamma\gamma}$, shown in Eqs. (8) and (9). Since we have $C_{\gamma\gamma}^{\rm eff}\approx C_{\gamma\gamma}+C_{\mu\mu}$, this modifies the ALP-decay branching ratio and the experiment constraints. We consider both of the ALP decays $a\to\mu^+\mu^-$ and $a\to\gamma\gamma$, which lead to the exotic Z decay final states as $(\mu^+\mu^-)\gamma$, $(\gamma\gamma)\gamma$, and $(\mu^+\mu^-)\mu^+\mu^-$. The relevant SM backgrounds are simulated using MadGraph5@NLO [73]. There is one more exotic decay $(\gamma\gamma)\mu^+\mu^-$ which is less covered by the experiments, we leave its phenomenology study to future work. The branching ratios of relevant decay modes $Z\to a\gamma$ and $Z\to a\mu^+\mu^-$ are given in Fig. 4 for $C_{WW}=0$, $m_a=5(50)$ GeV respectively. The exotic Z decay searches lead to strong constraints for $m_a<m_Z$, but the limits fade away when m_a close to m_Z. Therefore, we extend them to searches at Higgs factories with $\sqrt{s}=240$ GeV, based on s-channel production through off shell Z/γ, to cover $m_a>m_Z$.

To get a more realistic estimate, we impose some basic cuts [91] on the kinematics of the muons and photons in the final state to suppress the SM background. The opposite-sign

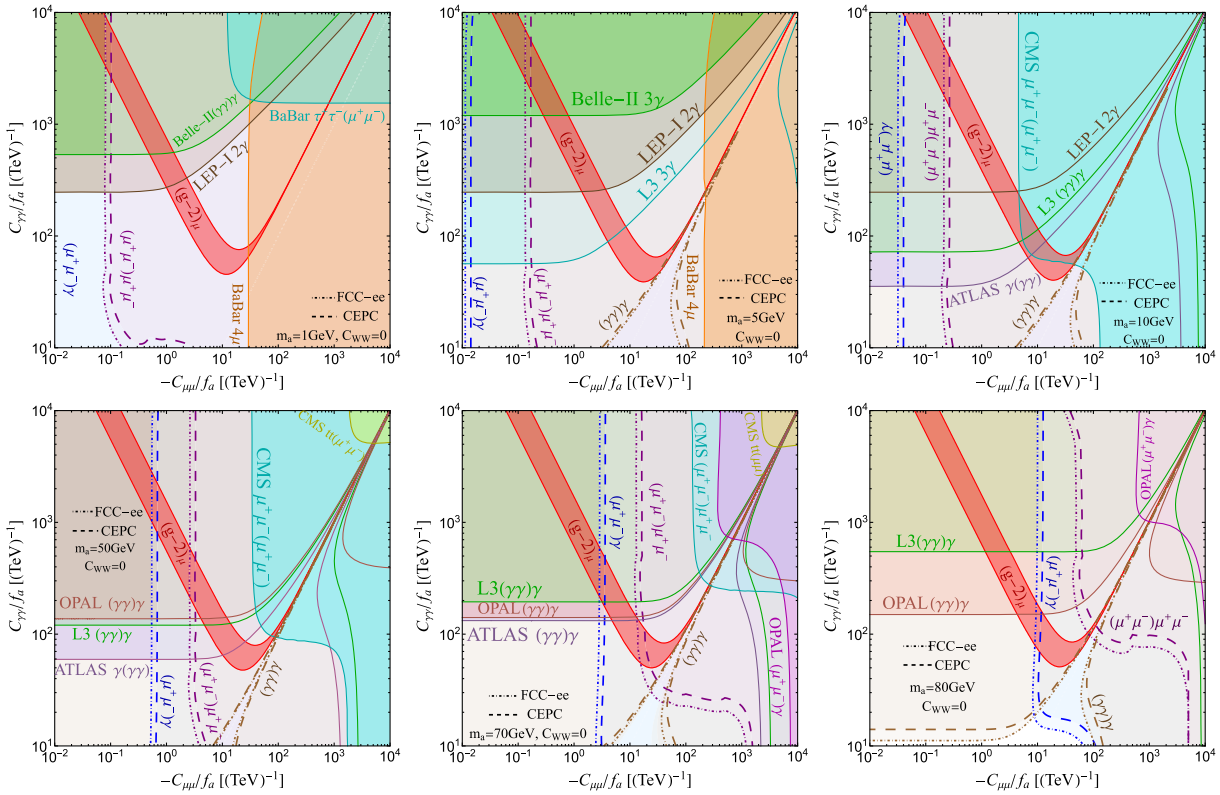

FIG. 8. The constraints from various existing experiments and future projections from Z factories (CEPC and FCC-ee) from exotic Z decay searches $Z \to a\gamma \to (\gamma\gamma)\gamma$, $Z \to a\gamma \to (\mu^+\mu^-)\gamma$, and $Z \to a\mu^+\mu^- \to (\mu^+\mu^-)\mu^+\mu^-$. The parameter space of $(g-2)_\mu$ solution is plotted in the red band. We set $C_{WW} = 0$, and $\Lambda = 1$ TeV in $g-2$ calculation.

muons are required to be spatially separated, $\Delta R > 0.1$. For $a \to \mu^+\mu^-$ decay, to take into account the resolution for the invariant mass of dimuon, we require $|m_{\mu\mu}/m_a - 1| < 0.19\%$. For $a \to \gamma\gamma$ decay, we require $|m_{\gamma\gamma} - m_a| < 1$ GeV, while in the $Z \to (\gamma\gamma)\gamma$ decay we further require the third photon form the Z resonance together with the first two photons [71]. We summarize the basic cuts and the specific requirements for each exotic Z decay channel in the following:

1. Basic cuts: $E_\gamma > 2$ GeV, $p_T^\mu > 0.1$ GeV, $|\eta_{\gamma/\mu}| < 3.0$

2. $Z \to (\mu^+\mu^-)\gamma$: $\left|\dfrac{m_{\mu\mu} - m_a}{m_a}\right| < 0.19\%$,

3. $Z \to (\gamma_1\gamma_2)\gamma_3$: $|m_{\gamma_1\gamma_2} - m_a| < 1$ GeV, $\left|E_{\gamma_3} - \dfrac{m_Z^2 - m_a^2}{2m_Z}\right| < 1$ GeV,

4. $Z \to (\mu^+\mu^-)\mu^+\mu^-$: at least one opposite sign muon pair $\left|\dfrac{m_{\mu\mu} - m_a}{m_a}\right| < 0.19\%$, $\Delta R_{\mu^+\mu^-} > 0.1$, $p_T^\mu > 5$ GeV. (26)

For a Higgs factory with $\sqrt{s} = 240$ GeV, we substitute m_Z in the above cuts to 240 GeV. The main results of our study, with the assumption of $C_{WW} = 0$, are shown in Figs. 8 and 9.

C. Summary of current limits and projected reach $C_{WW} = 0$

Based on the discussions in Secs. III A and III B, we summarize the current constraints and the projected reaches of Z factories (CEPC and FCC-ee).

Figure 8 shows the result on the ALP couplings $C_{\mu\mu}/f_a$ and $C_{\gamma\gamma}/f_a$, for different benchmark ALP masses. In particular, the results for $m_a = 1$, 5, 10, 50, 70, and 80 GeV are plotted. For light m_a and small $C_{\mu\mu}$, the parameter region capable of explaining the $(g-2)_\mu$ anomaly (red band) is constrained by $a\gamma \to (\gamma\gamma)\gamma$ from Belle-II [62], L3 [66], OPAL [63], and ATLAS [67] or inclusive $\gamma\gamma$ from LEP-I [65] searches. At the same time, for large $C_{\mu\mu}$, the decay channel to $a \to \mu^+\mu^-$ leads to

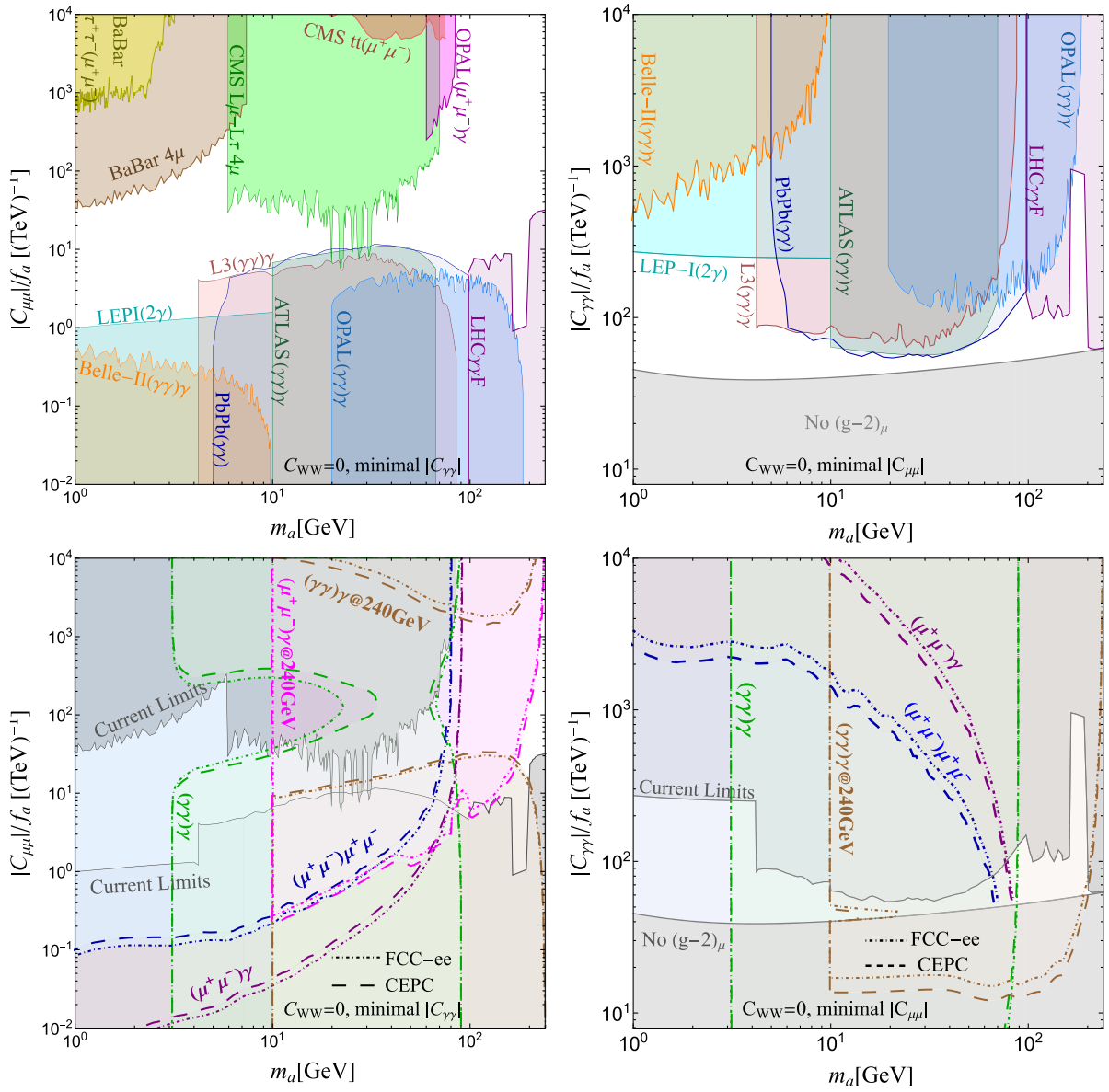

FIG. 9. Left panels: The existing constraints and future sensitivities in the $C_{\mu\mu}/f_a - m_a$ plane. We set $C_{WW} = 0$. For each pair of parameters, $C_{\mu\mu}$ and m_a, we choose the minimal $|C_{\gamma\gamma}|$ which can explain the $(g-2)_\mu$ anomaly at 2σ level. Right panels: The existing constraints and future sensitivities in the $C_{\gamma\gamma}/f_a - m_a$ plane with $C_{WW} = 0$. We choose the minimal $|C_{\mu\mu}|$ coupling which can satisfy $(g-2)_\mu$ anomaly at 2σ level. The gray region has no viable $g-2$ solution and we simply set $C_{\mu\mu} = 0$ here. Top panels: The existing constraints are plotted in color with the solid line as a boundary at 95% confidence level. Bottom panels: The reaches of future Z-factories at CEPC (dashed lines) and FCC-ee (dot-dashed lines) with searches $(\gamma\gamma)\gamma$, $(\mu^+\mu^-)\gamma$, and $(\mu^+\mu^-)\mu^+\mu^-$ are shown, while the reaches of the future Higgs factories are labeled with an extra @ 240 GeV.

constraints from *BABAR* $(\mu^+\mu^-)\mu^+\mu^-$ and $\tau^+\tau^- a \to \tau^+\tau^-(\mu^+\mu^-)$ searches [60,61]. For large m_a mass, the similar feature holds that the small $C_{\mu\mu}$ is constrained by 3γ or 2γ searches, while large $C_{\mu\mu}$ is constrained by axion-muonic decay searches. In contrast to the low m_a case, the CMS searches of $pp \to Z \to \mu^+\mu^-\phi$ and $pp \to \bar{t}t\phi$ [58,68] with ϕ decaying to muon pair come into play due to invariant mass threshold. The former requires the reconstruction of the Z boson from four-muon invariant mass. The latter does not require ϕ mass to be around m_Z, and its limit for a ϕ mass higher than Z is too weak to show up on the figure. The OPAL search $Z \to \mu^+\mu^-\gamma$ [64] is also relevant and complements the CMS limits.

For the range of m_a considered here, the limits from $3\gamma/2\gamma$ final states disappear for the right part of the $(g-2)_\mu$ band, where $C_{\gamma\gamma} + C_{\mu\mu} \sim 0$. This is because the BR$(a \to \gamma\gamma)$ is governed by $C_{\gamma\gamma}^{\text{eff}}$ in Eq. (8), which is vanishingly small in this case. This region is easily covered by

Z-factory searching for $Z \to (\mu^+\mu^-)\gamma$ and $Z \to (\mu^+\mu^-)\mu^+\mu^-$, which benefit from the vanishing $\mathrm{BR}(a \to \gamma\gamma)$. Together with $Z \to (\gamma\gamma)\gamma$, the Z-factory can cover the rest of the parameter space relevant for an explanation of the $(g-2)_\mu$ anomaly up to $m_a \lesssim 85$ GeV, providing a decisive check for the ALP solution to $(g-2)_\mu$ and is complementary to other existing experiments.

Figure 9 presents the existing constraints and future reaches in the $C_{\mu\mu}(C_{\gamma\gamma})/f_a - m_a$ plane, where we place the existing ones in the top panel and future ones in the bottom panel. To focus further on the relevant part of the parameter region, we will impose the condition that the parameter which is not plotted is chosen so that an explanation of the $(g-2)_\mu$ anomaly is possible. In the left panel, we choose $C_{\mu\mu}$ and m_a as free parameters, while $C_{\gamma\gamma}$ is chosen to be the minimal value which can give an explanation to the $(g-2)_\mu$ anomaly at 2σ level. In the right panel, we choose the minimal $C_{\mu\mu}$ in a similar way. The only exception is the gray region in the right panel where a possible explanation for the $(g-2)_\mu$ anomaly can not be found within the model under consideration.

In the left panel of Fig. 9, one might expect that a larger $C_{\gamma\gamma}$ could help to evade the $a \to \mu^+\mu^-$ searches via smaller branching ratio. However, this effect is compensated by the increased cross section of $e^+e^- \to a\mu^+\mu^-$ and $Z \to a\mu^+\mu^-$, because large $C_{\gamma\gamma,\gamma Z}$ will dominate the contribution comparing with $C_{\mu\mu}$. This feature is clear in Fig. 8 that the *BABAR* 4μ and Z-factory $a(\mu^+\mu^-)\gamma, a(\mu^+\mu^-)\mu^+\mu^-$ boundaries become vertical with increasing $C_{\gamma\gamma}$. The existing constraints leave the lower-half of the plot unconstrained. At the same time, the future probes from Z-factories can fully cover the parameter space up to $m_a \sim 85$ GeV.

The constraints from photon final states $(\gamma\gamma)\gamma$ set limits on the small $C_{\mu\mu}$ region, where a large $C_{\gamma\gamma}$ is necessary for explaining the $(g-2)_\mu$ anomaly. The constraints from the low-energy e^+e^- collider Belle-II [62], L3 [66] search based on Z-pole data, OPAL [63] search based on the data collected during the ~200 GeV run, pp collider Z study from ATLAS [67], photon fusion from PbPb ion collision [75,76] and pp collision at the LHC [77,78] are shown in the top-left panel. Together with $\mu^+\mu^-$, it still leaves the possibilities open for $|C_{\mu\mu}|/f_a \sim 10\ \mathrm{TeV}^{-1}$ for $m_a < m_Z$ and for $m_a > m_Z$ with large $C_{\mu\mu}$. Adding the constraints from exotic Z decays searches the Z-factory, one can fully cover the parameter space for $m_a < 85$ GeV. With the 240 GeV run, one can extend the exclusion up to $m_a \sim 160$ GeV via $e^+e^- \to (\gamma\gamma)\gamma$ and $(\mu^+\mu^-)\gamma$, which is complementary to the LHC studies. It can cover part of parameter region for m_a up to 240 GeV, but leaves a small opening for $|C_{\mu\mu}|/f_a \sim 10$–$100\ \mathrm{TeV}^{-1}$.

In the right panel of Fig. 9, for $C_{\gamma\gamma}$ within the "No $(g-2)_\mu$" band (gray region), there is no viable solutions and we set $C_{\mu\mu} = 0$ in this region by hand. The existing searches for $3\gamma/2\gamma$ multiphoton states have excluded a good portion of the parameter space in the top-right panel. The OPAL $(\gamma\gamma)\gamma$, photon fusion at Pb-Pb ion collision and pp collider searches at high energy can cover ALP masses larger than m_Z because they do not rely on the on shell Z. They leave an open space for $|C_{\gamma\gamma}|/f_a \sim 50$–$200\ \mathrm{TeV}^{-1}$. The future Z-factory probes can cover the parameter region for the ALP explanation to $(g-2)_\mu$ anomaly up to $m_a = 85$ GeV.

The $(\gamma\gamma)\gamma$ search from future Higgs factories can cover the higher mass region up to $m_a \sim 160$ GeV. One can see that the relevant parameter space is almost excluded.

D. Summary of constraints and projected reaches $C_{WW} \neq 0$

Our results on the ALP contribution to $(g-2)_\mu$ can be extended to cases with $C_{WW} \neq 0$ in a straightforward way. In this case, the couplings $C_{\gamma\gamma}$ and $C_{\gamma Z}$ are independent. There are four free parameters for the model, $m_a, C_{\mu\mu}, C_{WW}$, and C_{BB}. Since the 2-loop Barr-Zee diagram with W boson running in the loop is small compared with other diagrams, the C_{WW} contribution to $(g-2)_\mu$ comes mainly from the fact that it enters the independent $C_{\gamma\gamma}$ and $C_{\gamma Z}$ couplings.

Since we have more free parameters, it becomes difficult to present the full results in the two-dimensional plane. Instead, it is illuminating to present the results in $C_{BB}/f_a - C_{WW}/f_a$ parameter space for fixed values of $C_{\mu\mu}$ and m_a. In Fig. 10, we choose ALP masses $m_a = 5$, 10, 50, 70, and 100 GeV. For muon coupling, we choose small value of $C_{\mu\mu}/f_a = -5$ and $-50\ \mathrm{TeV}^{-1}$, respectively (for 10 GeV case, $C_{\mu\mu}/f_a = -50\ \mathrm{TeV}^{-1}$ is fully excluded by CMS 4μ search and we show $C_{\mu\mu}/f_a = -10\ \mathrm{TeV}^{-1}$ instead, and for 100 GeV, we choose $C_{\mu\mu}/f_a = -10\ \mathrm{TeV}^{-1}$) which can evade most of the constraints based on the searches for muonic final states. These values fall into the left branch in Fig. 2, which correspond to the small $C_{\mu\mu}$ solutions. For larger $C_{\mu\mu}$, the constraints from $3\gamma/2\gamma$ searches are less stringent, but the Z-factory search channel $\mu^+\mu^-\gamma$ could probe more parameter spaces, similar to the situation of $C_{WW} = 0$. The $(g-2)_\mu$ bands (red) in Fig. 10 have negative slope, corresponding to approximately constant $C_{\gamma\gamma}$. This implies that the contribution to $(g-2)_\mu$ is dominated by $C_{\gamma\gamma}$ coupling and the contribution from Z/W bosons is less important.

For general ALP-gauge couplings, the constraint from Z width precision measurement, Γ_Z^{tot}, should be taken into account. If $C_{WW} = 0$, this constraint is weaker than the one from exotic photon final-state searches. The Z total decay width measured by LEP is $\Gamma_Z^{\mathrm{tot}} = (2.495 \pm 0.0023)$ GeV [92]. It requires the BSM branching ratio $\mathrm{BR}(Z \to \mathrm{BSM}) < 0.0018$ at 95% C.L. It strictly limits the large C_{WW} values for small m_a, as shown in Fig. 10.

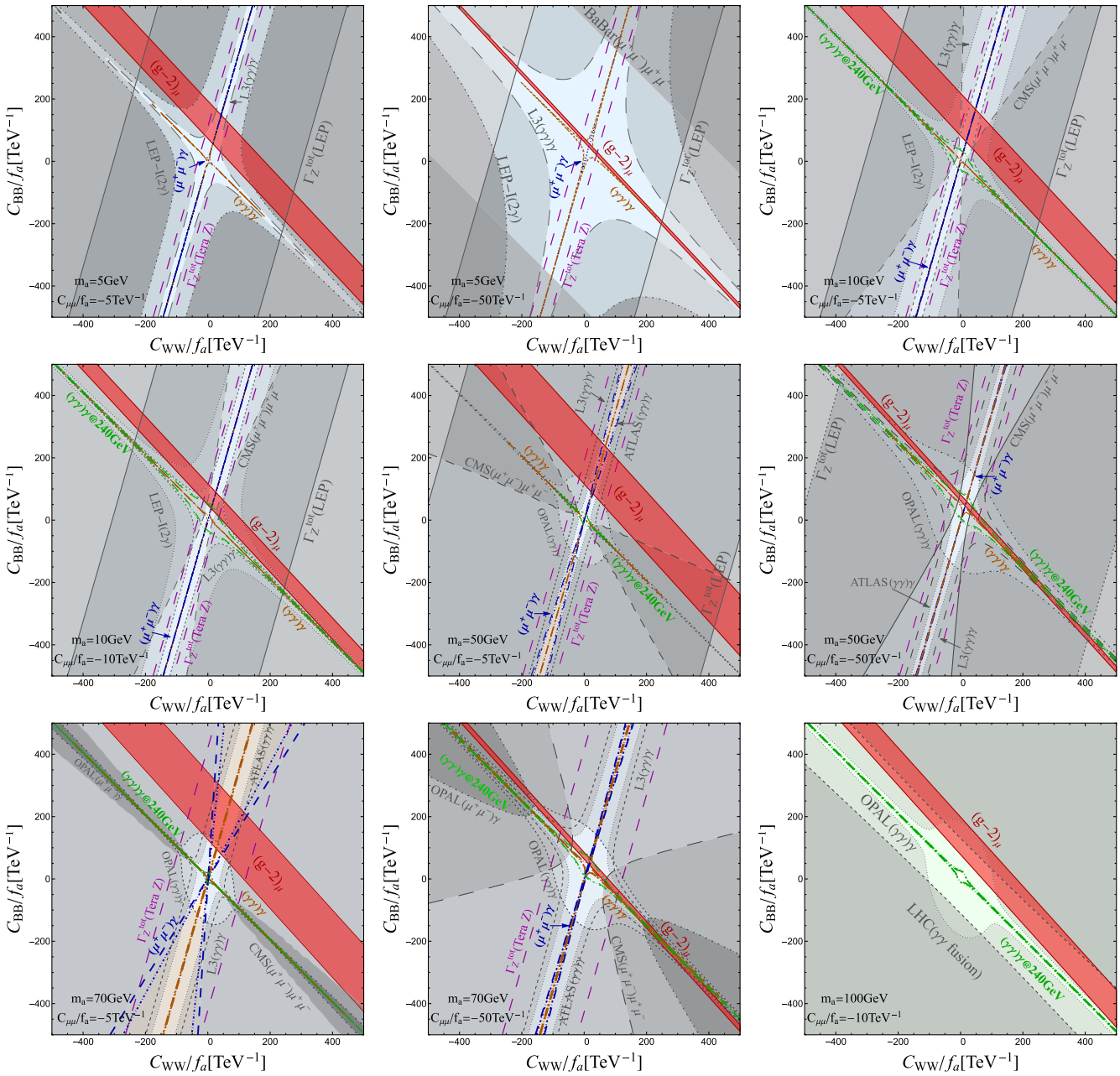

FIG. 10. The existing constraints and future sensitivities from Z-factory with $C_{WW} \neq 0$. The color codes are similar to Fig. 9. We choose $m_a = 5$, 10, 50, 70, 100 GeV, respectively together with appropriate small muon couplings $C_{\mu\mu}$.

The projected Tera-Z $\Gamma_Z^{\rm tot}$ measurement could further reduce the uncertainty to around 25 keV [84,93,94]. For $m_a \lesssim 5$ GeV, the flavor-violating meson exotic decay induced by nonzero C_{WW} strongly constrains the parameter space of ALP [55]. This constraint is absent for $m_a > 5$ GeV.

For $m_a = 5$ GeV, the most stringent existing constraints are the LEP-I ($Z \to 2\gamma$), L3 [$Z \to (\gamma\gamma)\gamma$] searches and the Γ_Z measurement. There is still a large portion of $(g-2)_\mu$ band which is not constrained but will be fully covered by Tera-$Z \to a\gamma \to (\mu^+\mu^-)\gamma$ except a small line presenting $C_{\gamma Z}^{\rm eff} \approx 0$. This is a general feature for exotic Z decay channel $Z \to a\gamma$.

For $m_a = 10$ GeV, more existing searches are relevant because the invariant mass is large enough to go above the dimuon threshold at the CMS $pp \to 4\mu$ search and the diphoton threshold at the L3 $Z \to 3\gamma$ search. The constraints from L3 $Z \to 3\gamma$ leaves a cross-shaped region open. The region with a positive slope corresponds to $C_{\gamma Z}^{\rm eff} \approx 0$ which minimizes the production cross section. There is also an unconstrained region with a negative slope since $C_{\gamma\gamma}^{\rm eff} \approx 0$ leads to vanishing branching ratio BR$(a \to \gamma\gamma)$.

The limits from LEP-I ($Z \to 2\gamma$) and the Z factory ($Z \to a\gamma \to 3\gamma$) searches share the same feature as those from L3. The former is weaker and less constraining, while the latter is very strong leaving open only the two (very fine-tuned) directions with $C^{\text{eff}}_{\gamma\gamma,\gamma Z} = 0$. The CMS $pp \to 4\mu$ search leaves a region open close to $C^{\text{eff}}_{\gamma Z} \approx 0$, since we have already chosen a pretty small $C_{\gamma\gamma}$ which means a large $C_{\gamma Z}$ is necessary to the production of $a\mu^+\mu^-$ final state. The Z-factory $Z \to a\gamma \to (\mu^+\mu^-)\gamma$ search shares similar feature that only the fine-tuned direction $C^{\text{eff}}_{\gamma Z} = 0$ is allowed. The green-shaded region in the plot shows the projection for the $(\gamma\gamma)\gamma$ @ 240 GeV channel. Since $e^+e^- \to a(\gamma\gamma)\gamma$ at $\sqrt{s} =$ 240 GeV is not close to the Z-pole, the projected coupling limit is much weaker than the $(\gamma\gamma)\gamma$ channel at the Z-pole, except in the fine-tuned case where $C^{\text{eff}}_{\gamma Z} \approx 0$. Additionally, for small masses such as $m_a = 10$ GeV, the branching ratio of $a \to \gamma\gamma$ is suppressed by m_a compared to $a \to \mu\mu$. Furthermore, the decayed γ from a light ALP has a lower chance of passing the energy-selection criteria. Therefore, the $(\gamma\gamma)\gamma$ @ 240 GeV channel has difficulty covering the $(g-2)_\mu$ region.

For $m_a = 50$ GeV, new constraints from the ATLAS $Z \to 3\gamma$ and the OPAL $ee \to 3\gamma$ searches become relevant. The former still leaves two fine-tuned directions open with $C^{\text{eff}}_{\gamma\gamma,\gamma Z} = 0$. The latter fully excludes the $C^{\text{eff}}_{\gamma Z} = 0$ direction since OPAL data were taken during runs at higher energy than m_Z. The signal does not vanish in $C^{\text{eff}}_{\gamma Z} = 0$ direction, because it can be generated via $C_{\gamma\gamma}$ alone, as shown in the second diagram of Fig. 5. Future $ee \to (\gamma\gamma)\gamma$ search at 240 GeV could also push forward on $C^{\text{eff}}_{\gamma Z} = 0$ direction limit.

For $m_a = 50$ GeV and 70 GeV, the Z-factory $Z \to a\gamma \to (\mu^+\mu^-)\gamma$ search leaves an open region with smaller $C_{\mu\mu}$ due to the smaller branching ratio of $a \to \mu^+\mu^-$. Similar to the case of $m_a = 10$ GeV, Z-factory ($Z \to a\gamma \to 3\gamma$) search is very powerful, leaving only two fine-tuned directions with $C^{\text{eff}}_{\gamma\gamma} = 0$ and $C^{\text{eff}}_{\gamma Z} = 0$.

For $m_a = 100$ GeV, the limits from on shell Z decay no longer apply. The OPAL $ee \to (\gamma\gamma)\gamma$ provides significant limits to the parameter space which covers the $C^{\text{eff}}_{\gamma Z} = 0$ direction. We show the LHC photon-fusion constraints ($\gamma\gamma$F) from Pb-Pb ion collision and pp collision which is complementary to OPAL limits. Since the LHC $\gamma\gamma$F constraints show similar limits comparing with OPAL, we only show their limits for $m_a = 100$ GeV for better readability. Future $ee \to (\gamma\gamma)\gamma$ search @ 240 GeV is shown as green-shaded region, which can cover the entire red $(g-2)_\mu$ band.

To summarize, in comparison with the minimal case, including the possibility of $C_{WW} \neq 0$ does not qualitatively change the picture. This is due to the fact that the contribution to $(g-2)_\mu$ is dominated by $C_{\gamma\gamma}$ coupling. The contributions from Z/W bosons are less relevant. With $C_{WW} \neq 0$, there are two new fine-tuned directions $C^{\text{eff}}_{\gamma\gamma,\gamma Z} = 0$, which help to evade limits from the exotic Z decays to photon final states. The Z-factory constraints are so powerful that the allowed points lie very close to a line with almost exact cancellation. Interestingly, the OPAL $ee \to (\gamma\gamma)\gamma$ search does not rely on on shell Z production, thus it can exclude $C^{\text{eff}}_{\gamma Z} = 0$ direction. In addition, this process can be applied to future Higgs factories at FCC-ee and CEPC running at $\sqrt{s} = 240$ GeV, which further excludes the parameter spaces for larger mass $m_a > m_Z$. Comparing $Z \to (\gamma\gamma)\gamma$ at future Z factories and $ee \to (\gamma\gamma)\gamma$ at Higgs factories, the number of signal events for the former are larger than the latter by about a factor of 100. Therefore, for $m_a < m_Z$, the limits are dominated by exotic Z decays except for mass threshold and fine-tuned directions.

IV. CONCLUSIONS

The deviation between the $(g-2)_\mu$ measurement and the SM prediction is a tantalizing sign of possible new physics beyond the Standard Model. A generic ALP with sizable couplings to muons and photons can provide a potential explanation for the $(g-2)_\mu$ anomaly. In this paper we start with ALP effective Lagrangian with general couplings to electroweak gauge fields and muons. We provide full $(g-2)_\mu$ calculations in ALP-fermion derivative coupling basis up to the 2-loop Barr-Zee diagrams. The importance of the inner-loop counterterm is addressed and we also provide an understanding of the existence of the inner-loop counterterm with chiral transformation in Eq. (25). We also extended the previous results by including heavy gauge boson Z and W into the calculation up to the 2-loop level, which is necessary due to the existence of counter terms and the heavy axion mass.

To recast the existing search results to our scenario, we performed simulations. In comparison with most of the previous studies, our scenario has the coupling between the ALP to both the muon and the gauge bosons. Some unique channels open up for this scenario. One such example is $Z \to \mu^+\mu^-\gamma$. In addition, we have updated the constraints from light particle searches, such as the CMS muonic force search [58], which can provide limits on the ALP model which has not been taken into account previously. Moreover, there are more Feynman diagrams involved in our scenario, the results in general can not be obtained by simple rescaling and signal simulation is necessary. We conclude that the existing results from experimental searches can place bounds on the parameter space relevant for an explanation of $(g-2)_\mu$ anomaly, but there is still a large open space.

As a powerful experimental probe of the ALP scenario, we propose to search for $(\gamma\gamma)\gamma$, $(\mu^+\mu^-)\gamma$ and $(\mu^+\mu^-)\mu^+\mu^-$ at future Tera-Z and Higgs factories, such as the CEPC and FCC-ee. They can be sensitive to parameter space relevant

for an $(g-2)_\mu$ explanation up to $m_a \sim 85$ GeV from exotic Z-decay searches, and the reach can be extended to ~160 GeV at future Higgs factories, which are complimentary to other existing experimental searches. We also include the C_{WW} coupling which is not considered before. In this case, the ratio $C_{\gamma Z}/C_{\gamma\gamma}$ is no longer fixed. Moreover, one of the couplings $C_{\gamma Z}, C_{\gamma\gamma}$ can become vanishingly small which can help to evade the existing bounds and even the future Z-factory's probes. One exception is the OPAL $(\gamma\gamma)\gamma$ search at energies between 181–209 GeV [63] which can constrain the fine-tuned direction $C_{\gamma Z} = 0$. Future Higgs factories such as FCC-ee and CEPC running at 240 GeV can further exclude the parameter space up to $m_a \sim 160$ GeV through $(\gamma\gamma)\gamma$ and $(\mu^+\mu^-)\gamma$ channels.

ACKNOWLEDGMENTS

We would like to thank JiJi Fan for the helpful discussions. The work of J. L. is supported by the National Science Foundation of China under Grants No. 12075005 and No. 12235001, and by Peking University under startup Grant No. 7101502458. The work of X. P. W. is supported by the National Science Foundation of China under Grant No. 12005009. L. T. W. is supported by the DOE Grant No. DE-SC0013642.

[1] R. J. Crewther, P. Di Vecchia, G. Veneziano, and E. Witten, Chiral estimate of the electric dipole moment of the neutron in quantum chromodynamics, Phys. Lett. **88B**, 123 (1979); **91B**, 487(E) (1980).
[2] G. Pignol and P. Schmidt-Wellenburg (nEDM Collaboration), The search for the neutron electric dipole moment at PSI, SciPost Phys. Proc. **5**, 027 (2021).
[3] R. Golub and K. Lamoreaux, Neutron electric dipole moment, ultracold neutrons and polarized ^{3}He, Phys. Rep. **237**, 1 (1994).
[4] C. Abel *et al.*, Measurement of the Permanent Electric Dipole Moment of the Neutron, Phys. Rev. Lett. **124**, 081803 (2020).
[5] R. D. Peccei and H. R. Quinn, *CP* Conservation in the Presence of Instantons, Phys. Rev. Lett. **38**, 1440 (1977).
[6] R. D. Peccei and H. R. Quinn, Constraints imposed by *CP* conservation in the presence of instantons, Phys. Rev. D **16**, 1791 (1977).
[7] S. Weinberg, A New Light Boson?, Phys. Rev. Lett. **40**, 223 (1978).
[8] F. Wilczek, Problem of Strong P and T Invariance in the Presence of Instantons, Phys. Rev. Lett. **40**, 279 (1978).
[9] C. Vafa and E. Witten, Parity Conservation in QCD, Phys. Rev. Lett. **53**, 535 (1984).
[10] G. G. Raffelt, Astrophysical methods to constrain axions and other novel particle phenomena, Phys. Rep. **198**, 1 (1990).
[11] L. D. Duffy and K. van Bibber, Axions as dark matter particles, New J. Phys. **11**, 105008 (2009).
[12] M. Kawasaki and K. Nakayama, Axions: Theory and cosmological role, Annu. Rev. Nucl. Part. Sci. **63**, 69 (2013).
[13] D. J. E. Marsh, Axion cosmology, Phys. Rep. **643**, 1 (2016).
[14] P. W. Graham, I. G. Irastorza, S. K. Lamoreaux, A. Lindner, and K. A. van Bibber, Experimental searches for the axion and axion-like particles, Annu. Rev. Nucl. Part. Sci. **65**, 485 (2015).
[15] M. Bauer, M. Neubert, and A. Thamm, Collider probes of axion-like particles, J. High Energy Phys. 12 (2017) 044.
[16] L. Di Luzio, M. Giannotti, E. Nardi, and L. Visinelli, The landscape of QCD axion models, Phys. Rep. **870**, 1 (2020).
[17] V. Andreev *et al.* (ACME Collaboration), Improved limit on the electric dipole moment of the electron, Nature (London) **562**, 355 (2018).
[18] G. W. Bennett *et al.* (Muon (g-2) Collaboration), An improved limit on the muon electric dipole moment, Phys. Rev. D **80**, 052008 (2009).
[19] D. Hanneke, S. Fogwell, and G. Gabrielse, New Measurement of the Electron Magnetic Moment and the Fine Structure Constant, Phys. Rev. Lett. **100**, 120801 (2008).
[20] D. Hanneke, S. F. Hoogerheide, and G. Gabrielse, Cavity control of a single-electron quantum cyclotron: Measuring the electron magnetic moment, Phys. Rev. A **83**, 052122 (2011).
[21] T. Aoyama *et al.*, The anomalous magnetic moment of the muon in the standard model, Phys. Rep. **887**, 1 (2020).
[22] G. W. Bennett *et al.* (Muon g-2 Collaboration), Final report of the muon E821 anomalous magnetic moment measurement at BNL, Phys. Rev. D **73**, 072003 (2006).
[23] B. Abi *et al.* (Muon g-2 Collaboration), Measurement of the Positive Muon Anomalous Magnetic Moment to 0.46 ppm, Phys. Rev. Lett. **126**, 141801 (2021).
[24] M. Davier, A. Hoecker, B. Malaescu, and Z. Zhang, Reevaluation of the hadronic contributions to the muon g-2 and to alpha(MZ), Eur. Phys. J. C **71**, 1515 (2011); **72**, 1874(E) (2012).
[25] T. Aoyama, M. Hayakawa, T. Kinoshita, and M. Nio, Complete Tenth-Order QED Contribution to the Muon $g-2$, Phys. Rev. Lett. **109**, 111808 (2012).
[26] T. Aoyama, T. Kinoshita, and M. Nio, Theory of the anomalous magnetic moment of the electron, Atoms **7**, 28 (2019).
[27] A. Czarnecki, W. J. Marciano, and A. Vainshtein, Refinements in electroweak contributions to the muon anomalous magnetic moment, Phys. Rev. D **67**, 073006 (2003); **73**, 119901(E) (2006).
[28] C. Gnendiger, D. Stöckinger, and H. Stöckinger-Kim, The electroweak contributions to $(g-2)_\mu$ after the Higgs boson mass measurement, Phys. Rev. D **88**, 053005 (2013).

[29] M. Davier, A. Hoecker, B. Malaescu, and Z. Zhang, Reevaluation of the hadronic vacuum polarisation contributions to the standard model predictions of the muon $g-2$ and $\alpha(m_Z^2)$ using newest hadronic cross-section data, Eur. Phys. J. C **77**, 827 (2017).
[30] A. Keshavarzi, D. Nomura, and T. Teubner, Muon $g-2$ and $\alpha(M_Z^2)$: A new data-based analysis, Phys. Rev. D **97**, 114025 (2018).
[31] G. Colangelo, M. Hoferichter, and P. Stoffer, Two-pion contribution to hadronic vacuum polarization, J. High Energy Phys. 02 (2019) 006.
[32] M. Hoferichter, B.-L. Hoid, and B. Kubis, Three-pion contribution to hadronic vacuum polarization, J. High Energy Phys. 08 (2019) 137.
[33] M. Davier, A. Hoecker, B. Malaescu, and Z. Zhang, A new evaluation of the hadronic vacuum polarisation contributions to the muon anomalous magnetic moment and to $\boldsymbol{\alpha(m_Z^2)}$, Eur. Phys. J. C **80**, 241 (2020); **80**, 410(E) (2020).
[34] A. Keshavarzi, D. Nomura, and T. Teubner, The $g-2$ of charged leptons, $\alpha(M_Z^2)$ and the hyperfine splitting of muonium, Phys. Rev. D **101**, 014029 (2020).
[35] A. Kurz, T. Liu, P. Marquard, and M. Steinhauser, Hadronic contribution to the muon anomalous magnetic moment to next-to-next-to-leading order, Phys. Lett. B **734**, 144 (2014).
[36] K. Melnikov and A. Vainshtein, Hadronic light-by-light scattering contribution to the muon anomalous magnetic moment revisited, Phys. Rev. D **70**, 113006 (2004).
[37] P. Masjuan and P. Sánchez-Puertas, Pseudoscalar-pole contribution to the $(g_\mu-2)$: A rational approach, Phys. Rev. D **95**, 054026 (2017).
[38] G. Colangelo, M. Hoferichter, M. Procura, and P. Stoffer, Dispersion relation for hadronic light-by-light scattering: Two-pion contributions, J. High Energy Phys. 04 (2017) 161.
[39] M. Hoferichter, B.-L. Hoid, B. Kubis, S. Leupold, and S. P. Schneider, Dispersion relation for hadronic light-by-light scattering: Pion pole, J. High Energy Phys. 10 (2018) 141.
[40] A. Gérardin, H. B. Meyer, and A. Nyffeler, Lattice calculation of the pion transition form factor with $N_f=2+1$ Wilson quarks, Phys. Rev. D **100**, 034520 (2019).
[41] J. Bijnens, N. Hermansson-Truedsson, and A. Rodríguez-Sánchez, Short-distance constraints for the HLbL contribution to the muon anomalous magnetic moment, Phys. Lett. B **798**, 134994 (2019).
[42] G. Colangelo, F. Hagelstein, M. Hoferichter, L. Laub, and P. Stoffer, Longitudinal short-distance constraints for the hadronic light-by-light contribution to $(g-2)_\mu$ with large-N_c Regge models, J. High Energy Phys. 03 (2020) 101.
[43] T. Blum, N. Christ, M. Hayakawa, T. Izubuchi, L. Jin, C. Jung, and C. Lehner, The Hadronic Light-by-Light Scattering Contribution to the Muon Anomalous Magnetic Moment from Lattice QCD, Phys. Rev. Lett. **124**, 132002 (2020).
[44] G. Colangelo, M. Hoferichter, A. Nyffeler, M. Passera, and P. Stoffer, Remarks on higher-order hadronic corrections to the muon $g-2$, Phys. Lett. B **735**, 90 (2014).
[45] S. Borsanyi *et al.*, Leading hadronic contribution to the muon magnetic moment from lattice QCD, Nature (London) **593**, 51 (2021).
[46] M. Cè *et al.*, Window observable for the hadronic vacuum polarization contribution to the muon $g-2$ from lattice QCD, Phys. Rev. D **106**, 114502 (2022).
[47] D. Chang, W.-F. Chang, C.-H. Chou, and W.-Y. Keung, Large two loop contributions to g-2 from a generic pseudoscalar boson, Phys. Rev. D **63**, 091301 (2001).
[48] A. Dedes and H. E. Haber, Can the Higgs sector contribute significantly to the muon anomalous magnetic moment?, J. High Energy Phys. 05 (2001) 006.
[49] J. F. Gunion, A light *CP*-odd Higgs boson and the muon anomalous magnetic moment, J. High Energy Phys. 08 (2009) 032.
[50] W. J. Marciano, A. Masiero, P. Paradisi, and M. Passera, Contributions of axionlike particles to lepton dipole moments, Phys. Rev. D **94**, 115033 (2016).
[51] M. Bauer, M. Heiles, M. Neubert, and A. Thamm, Axion-like particles at future colliders, Eur. Phys. J. C **79**, 74 (2019).
[52] C. Cornella, P. Paradisi, and O. Sumensari, Hunting for ALPs with lepton flavor violation, J. High Energy Phys. 01 (2020) 158.
[53] M. Bauer, M. Neubert, S. Renner, M. Schnubel, and A. Thamm, Axionlike Particles, Lepton-Flavor Violation, and a New Explanation of a_μ and a_e, Phys. Rev. Lett. **124**, 211803 (2020).
[54] M. A. Buen-Abad, J. Fan, M. Reece, and C. Sun, Challenges for an axion explanation of the muon $g-2$ measurement, J. High Energy Phys. 09 (2021) 101.
[55] M. Bauer, M. Neubert, S. Renner, M. Schnubel, and A. Thamm, Flavor probes of axion-like particles, arXiv:2110.10698.
[56] The CEPC Study Group, Cepc conceptual design report: Volume 2—physics and detector (2018), https://arxiv.org/abs/1811.10545.
[57] A. Abada *et al.* (FCC Collaboration), FCC-ee: The lepton collider: Future circular collider conceptual design report volume 2, Eur. Phys. J. Special Topics **228**, 261 (2019).
[58] A. M. Sirunyan *et al.* (CMS Collaboration), Search for an $L_\mu-L_\tau$ gauge boson using $Z\to 4\mu$ events in proton-proton collisions at $\sqrt{s}=13$ TeV, Phys. Lett. B **792**, 345 (2019).
[59] P. S. B. Dev, R. N. Mohapatra, and Y. Zhang, Lepton Flavor Violation Induced by a Neutral Scalar at Future Lepton Colliders, Phys. Rev. Lett. **120**, 221804 (2018).
[60] J. P. Lees *et al.* (*BABAR* Collaboration), Search for a Dark Leptophilic Scalar in e^+e^- Collisions, Phys. Rev. Lett. **125**, 181801 (2020).
[61] J. P. Lees *et al.* (*BABAR* Collaboration), Search for a muonic dark force at *BABAR*, Phys. Rev. D **94**, 011102 (2016).
[62] F. Abudinén *et al.* (Belle-II Collaboration), Search for Axion-Like Particles Produced in e^+e^- Collisions at Belle II, Phys. Rev. Lett. **125**, 161806 (2020).
[63] G. Abbiendi *et al.* (OPAL Collaboration), Multiphoton production in $e+\ e-$ collisions at $s**(1/2)=181$-GeV to 209-GeV, Eur. Phys. J. C **26**, 331 (2003).
[64] P. D. Acton *et al.* (OPAL Collaboration), A Measurement of photon radiation in lepton pair events from Z0 decays, Phys. Lett. B **273**, 338 (1991).
[65] J. Jaeckel and M. Spannowsky, Probing MeV to 90 GeV axion-like particles with LEP and LHC, Phys. Lett. B **753**, 482 (2016).

[66] M. Acciarri *et al.* (L3 Collaboration), Search for anomalous $Z \to \gamma\gamma\gamma$events at LEP, Phys. Lett. B **345**, 609 (1995).
[67] G. Aad *et al.* (ATLAS Collaboration), Search for new phenomena in events with at least three photons collected in pp collisions at $\sqrt{s} = 8$ TeV with the ATLAS detector, Eur. Phys. J. C **76**, 210 (2016).
[68] A. M. Sirunyan *et al.* (CMS Collaboration), Search for physics beyond the standard model in multilepton final states in proton-proton collisions at $\sqrt{s} = 13$ TeV, J. High Energy Phys. 03 (2020) 051.
[69] H. H. Patel, Package-X: A mathematica package for the analytic calculation of one-loop integrals, Comput. Phys. Commun. **197**, 276 (2015).
[70] V. Ilisie, New Barr-Zee contributions to $(g-2)_\mu$ in two-Higgs-doublet models, J. High Energy Phys. 04 (2015) 077.
[71] J. Liu, L.-T. Wang, X.-P. Wang, and W. Xue, Exposing the dark sector with future Z factories, Phys. Rev. D **97**, 095044 (2018).
[72] S. Knapen, T. Lin, H. K. Lou, and T. Melia, Searching for Axionlike Particles with Ultraperipheral Heavy-Ion Collisions, Phys. Rev. Lett. **118**, 171801 (2017).
[73] J. Alwall, R. Frederix, S. Frixione, V. Hirschi, F. Maltoni, O. Mattelaer, H. S. Shao, T. Stelzer, P. Torrielli, and M. Zaro, The automated computation of tree-level and next-to-leading order differential cross sections, and their matching to parton shower simulations, J. High Energy Phys. 07 (2014) 079.
[74] A. Alloul, N. D. Christensen, C. Degrande, C. Duhr, and B. Fuks, FeynRules 2.0—A complete toolbox for tree-level phenomenology, Comput. Phys. Commun. **185**, 2250 (2014).
[75] A. M. Sirunyan *et al.* (CMS Collaboration), Evidence for light-by-light scattering and searches for axion-like particles in ultraperipheral PbPb collisions at $\sqrt{s_{\mathrm{NN}}} = 5.02$ TeV, Phys. Lett. B **797**, 134826 (2019).
[76] G. Aad *et al.* (ATLAS Collaboration), Measurement of light-by-light scattering and search for axion-like particles with 2.2 nb^{-1} of $\mathrm{Pb}+\mathrm{Pb}$ data with the ATLAS detector, J. High Energy Phys. 11 (2021) 050.
[77] A. Tumasyan *et al.* (CMS, TOTEM Collaboration), First Search for Exclusive Diphoton Production at High Mass with Tagged Protons in Proton-Proton Collisions at $\sqrt{s} = 13$ TeV, Phys. Rev. Lett. **129**, 011801 (2022).
[78] S. Chatrchyan *et al.* (CMS Collaboration), Search for exclusive or semi-exclusive photon pair production and observation of exclusive and semi-exclusive electron pair production in pp collisions at $\sqrt{s} = 7$ TeV, J. High Energy Phys. 11 (2012) 080.
[79] P. Agrawal *et al.*, Feebly-interacting particles: FIPs 2020 workshop report, Eur. Phys. J. C **81**, 1015 (2021).
[80] M. Ahmad *et al.*, CEPC-SPPC preliminary conceptual design report. 1. Physics and detector.
[81] J. Beacham *et al.*, Physics beyond colliders at CERN: Beyond the standard model working group report, J. Phys. G **47**, 010501 (2020).
[82] A. Blondel *et al.*, Standard model theory for the FCC-ee Tera-Z stage, in *Proceedings of the Mini Workshop on Precision EW and QCD Calculations for the FCC Studies: Methods and Techniques*, CERN Yellow Reports: Monographs (CERN, Geneva, 2018), Vol. 3/2019, 9.
[83] J. Gao (CEPC Accelerator Study Group), Snowmass2021 White Paper AF3-CEPC, arXiv:2203.09451.
[84] G. Bernardi *et al.*, The future circular collider: A summary for the US 2021 snowmass process, arXiv:2203.06520.
[85] J. Liu, X.-P. Wang, and F. Yu, A tale of two portals: Testing light, hidden new physics at future e^+e^- colliders, J. High Energy Phys. 06 (2017) 077.
[86] M. Jin and Y. Gao, Z-pole test of effective dark matter diboson interactions at the CEPC, Eur. Phys. J. C **78**, 622 (2018).
[87] W.-F. Chang, J. N. Ng, and G. White, Prospects for detecting light bosons at the FCC-ee and CEPC, Phys. Rev. D **97**, 115015 (2018).
[88] Z. S. Wang and K. Wang, Long-lived light neutralinos at future Z-factories, Phys. Rev. D **101**, 115018 (2020).
[89] H.-C. Cheng, L. Li, E. Salvioni, and C. B. Verhaaren, Light hidden mesons through the Z portal, J. High Energy Phys. 11 (2019) 031.
[90] G. Cacciapaglia, A. Deandrea, A. M. Iyer, and K. Sridhar, Tera-Z stage at future colliders and light composite axion-like particles, Phys. Rev. D **105**, 015020 (2022).
[91] C. Chen, X. Mo, M. Selvaggi, Q. Li, G. Li, M. Ruan, and X. Lou, Fast simulation of the CEPC detector with Delphes, arXiv:1712.09517.
[92] S. Schael *et al.* (ALEPH, DELPHI, L3, OPAL, SLD Collaborations, LEP Electroweak Working Group, SLD Electroweak Group, SLD Heavy Flavour Group), Precision electroweak measurements on the Z resonance, Phys. Rep. **427**, 257 (2006).
[93] J. Alcaraz Maestre, A. Blondel, M. Dam, and P. Janot, The Z lineshape challenge: ppm and keV measurements, Eur. Phys. J. Plus **136**, 848 (2021).
[94] H. Cheng *et al.* (CEPC Physics Study Group), The physics potential of the CEPC. Prepared for the US Snowmass Community Planning Exercise (Snowmass 2021), in 2022 Snowmass Summer Study (2022), 5, arXiv:2205.08553.